Search for Rotational Symmetry of Binary Images via Radon Transform and Fourier Analysis

Nikita Lomov[1,2] [a], Oleg Seredin[3] [b], Olesia Kushnir[3] [c] and Daniil Liakhov[3] [d]

[1]*Office of Research and Development, Tula State University, Tula, Russian Federation*

[2]*Complex Systems Department, Federal Research Center "Computer Science and Control" of the Russian Federation Academy of Sciences, Moscow, Russia*

[3]*Cognitive Technologies and Simulation Systems Lab, Tula State University, Tula, Russian Federation*

Keywords: Rotational Symmetry, Jaccard Index, Affine Transformations, Radon Transform, Fourier Transform.

Abstract: We considered the optimization of such rotational symmetry properties in 2D shapes as the focus position, symmetry degree, and measure expressed as the Jaccard index generalized to a group of two or more shapes. We proposed to reduce the symmetry detection to the averaging of Jaccard indices for all possible pairs of rotated shapes. It is sufficient to consider a number of pairs linearly proportional to the degree of symmetry. It is shown that for a class of plane affine transformations translating lines into lines, and rotations in particular, the upper estimate of the Jaccard index can be directly derived from the Radon transform of the shape. We proposed a fast estimation of the shape degree of symmetry by applying the Fourier analysis of the secondary features derived from the Radon transform. The proposed methods were implemented as a highly efficient computational procedure. The results are consistent with the expert judgment of the qualities of symmetry.

1 INTRODUCTION

Detection of symmetrical objects is important for visual information processing by both humans and computers. It is also widely used in many manufacturing processes. It is significantly faster and cheaper to weld plastic parts by a laser when they are symmetric. The processing and storage of symmetric shapes in computer graphics applications can be greatly simplified. In environmental studies, the asymmetry factor of plant leaves is a good environmental health metric.

Rotational and reflectional symmetries are the most common types and most familiar to humans. Many rotational symmetry detection problem statements were considered. They differ in the quality criteria used to find the best points of rotation, shape parameterization approaches, and processing either the contour or interior of the shape.

The detection of reflectional and rotational symmetry in weak perspective projection images was proposed in (Lei and Wong, 1999). The method uses the Hough transform to detect the skewed symmetric axes and their skew angles. For each of the detected skewed axes and their angles an equation for the reflectional and rotational symmetry estimation was obtained. The Hough transform concepts were further advanced in (Yip, 1999), where the groups of symmetric points, i.e., coinciding with each other as they rotate in parallel projections, are considered. When the initial points in the groups are known, the author identifies the subsequent points and the group's focus of symmetry with geometric invariants. With multiple Hough transforms, the symmetry focus, parallel projection properties, and degree of symmetry are consistently determined as values found in most groups. Another work (Yip, 2007) describes a genetic Fourier descriptor for rotational symmetry detection. A closed curve can be represented by a periodic function or a set of the function's Fourier coefficients. The genetic algorithm is used to fit the coefficients to the solution. The resulting function is analyzed to find the rotational symmetry.

Symmetry detection by analyzing object contour chains consisting of small segments was described in (Aguilar et al., 2020). The chains are divided into fragments to be compared to detect the symmetry. The method offers excellent performance for detecting the object symmetry and its order, and good performance when handling quasi-symmetric objects.

[a] https://orcid.org/0000-0003-4286-1768

[b] https://orcid.org/0000-0003-0410-7705

[c] https://orcid.org/0000-0001-7879-9463

[d] https://orcid.org/0000-0003-1105-9780

Another contour-based approach (Llados et al., 1997) represents the shape boundary as substrings and subsequently uses their cyclic comparison to detect rotational symmetry. The key concept is that the boundary of a rotationally symmetric shape consists of identical substrings. The number of such substrings indicates the degree of rotational symmetry. The method works fine for perfect shapes, but requires adjusting the distortion factor when handling quasi-symmetric objects. A correlation measure to find various types of symmetry is used in (Kondra et al., 2013). The measure's maximum value characterizes the symmetry region. This approach makes it possible to search for symmetries even when there are multiple objects in the image. It was proposed in (Lee and Liu, 2010) to analyze the patterns occurring as the polar coordinate system with its origin at the possible center of symmetry is converted into a Cartesian coordinate system with the Fourier analysis.

Symmetry detection in full-color and grayscale images are also of considerable interest. The analysis of a so-called Gradient Vector Flow image was proposed in (Shiv Naga Prasad and Davis, 2005). A graph linking the image pixels similar to the rotated versions of each other in terms of the flow is generated. A presence of n-size cycles in the graph indicates the presence of a n-degree symmetry with its focus at the mean of cycle points. There are neural network-based rotational symmetry detection methods. A notable example of such an approach (Krippendorf and Syvaeri, 2020) assumes that the points symmetrical with respect to a complex transformation will have similar representation in the last hidden layer. It is also possible to develop special layers for neural networks in order to make these networks partially equivariant to rotations (Dieleman et al., 2016).

For this work, symmetry detection algorithms based on image projections are especially relevant. They consider not individual points, but groups of points behaving similarly during the transformation. The illustrative approach (Nguyen, 2019) uses a Radon transform of a 2D shape and its derivative R-signature as an integral over the squared Radon transform. The method core is the obvious consideration that the Radon transform along the lines parallel to the symmetry axis is also symmetric. The author further expanded this approach in (Nguyen et al., 2022), providing a large theoretical background and presenting a new binary image dataset to assess the symmetry detection strategies. This study uses the so-called LIP (the Largest Intersection and Projection) proposed in (Nguyen and Nguyen, 2018). It is a function of the angle expressing the ratio of the largest intersection with a shape selected from all the lines having a given angular direction to the shape's projection onto a perpendicular straight line.

These works deal with reflection symmetry, but similar theorems about the properties of symmetric shapes can be also derived for rotational symmetry. Note that although the above-mentioned works contain some important insights concerning the properties of symmetric shapes, for non-strict symmetry we face a problem of selecting from a set of "non-ideal" lines. We should somehow compare such lines with each other. The answer usually relies on statistical (e.g., the χ^2 criterion) or computationally defined (the Hough accumulator array analysis) criteria with no explicit geometric interpretation. Subsequently we will show that this problem can be solved by using the Jaccard index, a special shape comparison measure. The Radon transform applied to it produces explicit upper estimates of the measure and gives an upper approximation of the function to be optimized.

2 ROTATIONAL SYMMETRY MEASURE BASED ON THE JACCARD INDEX

In a strict sense, a planar shape A has a degree $k \geq 2$ rotational symmetry with its focus at $c = (x_c, y_c)$ if the shape does not change when rotated around the focus by $\{\frac{2\pi i}{k}\}_{i=1}^{k-1}$ angles. In other words, we can assume that we have a set of k shapes $\{A_0, \ldots A_{k-1}\}$, where the shape A_i is obtained from the shape A by rotating it by $\frac{2\pi i}{k}$. The symmetry criterion is that all these shapes coincide with each other. However, despite its exceptional value for geometry and group theory, such a definition is hardly applicable to the recognition of real-world images. There are two reasons for this. First, such objects are rare. The second reason is the ways images are stored in computer memory and the transformation algorithms are implemented. For instance, rotations of a raster image around a given point, generally speaking, do not generate a group. Moreover, for real-world applications we need not just to divide shapes in the images into "symmetrical" and "asymmetrical" ones, but to quantitatively estimate the symmetry measure as closeness to an absolutely symmetrical standard for all shapes, including those that are unambiguously estimated as asymmetrical in terms of common sense.

A symmetry measure based on Jaccard index (Kushnir et al., 2017) is of particular interest for the reflection symmetry analysis. The shape A is compared to its version A' reflected from its symmetry

axis:

$$J(A) = \frac{|A \cap A'|}{|A \cup A'|}. \quad (1)$$

This value range is $[0,1]$, which meets the definition of a measure. We will call the shapes quasi-symmetric if their symmetry measure is close to 1. Such a measure can be applied to degree 2 rotational (central) symmetry, since only two shapes are compared. The paper (Seredin et al., 2022) investigates the search for the symmetry focus point where the Jaccard index as a function of the focus position is approximated by a quadratic function, and then the search covers the neighborhood of the paraboloid vertex.

As the Jaccard index is generalized to rotational symmetry of any degree, more than two shapes are to be compared. An obvious solution would be to average the measures over all possible pairs:

$$J^{(k)}(A) = \frac{2}{k(k-1)} \sum_{i=0}^{k-2} \sum_{j=i+1}^{k-1} \frac{|A_i \cap A_j|}{|A_i \cup A_j|} =$$
$$= \frac{2}{k(k-1)} \sum_{i=0}^{k-2} \sum_{j=i+1}^{k-1} J_{ij}(A). \quad (2)$$

At first glance, this requires to process $\frac{k(k-1)}{2}$ number of pairs quadratic in k, which will negatively affect the computational efficiency. The following theorem shows that it is sufficient to consider a number of pairs linearly proportional to k.

Theorem 1. Let $\min(|i-j|, k-|i-j|) = \min(|p-q|, k-|p-q|)$ for $0 \le i, j, p, q \le k-1$. Then $|A_i \cap A_j| = |A_p \cap A_q|$, and $|A_i \cup A_j| = |A_p \cup A_q|$.

Proof. It follows that either $q \equiv_k p + (j-i)$, or $q \equiv_k p - (j-i)$ and $p \equiv_k q + (j-i)$. In the first case, A_p is obtained from A_i by rotating it by $\frac{2\pi(p-i)}{k}$, and A_q is obtained from A_j by rotating it by same angle around the same point. Therefore, $A_p \cap A_q$ and $A_p \cup A_q$ are obtained from $A_i \cap A_j$ and $A_i \cup A_j$ respectively by the same rotation, and the areas of these sets are maintained. The equality of areas in the second case follows from the commutativity of the intersection and union operations, so we can swap p and q. $\square$

It is sufficient to consider a pair of shape numbers (i,j) for each $d = \min(|i-j|, k-|i-j|)$, $1 \le d \le \frac{k}{2}$, for example, $(0,d)$ pairs. Let us introduce the coefficients into the final equation. For convenience, the pairs (i,j) and (j,i) are assumed to be identical, and modulo k numbers are processed. If $d < \frac{k}{2}$, each $(0,d)$ pair covers k of the original pairs: $(0,d), (1,d+1), \ldots (k-1, k-1+d)$. When $d = \frac{k}{2}$, the pair $(0,d)$ covers $\frac{k}{2}$ of the original pairs:

$$J(A_0, A_1) = 0.8223 \qquad J(A_0, A_2) = 0.8110$$
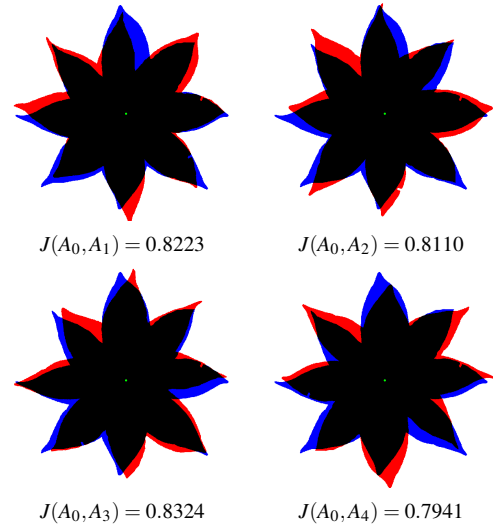
$$J(A_0, A_3) = 0.8324 \qquad J(A_0, A_4) = 0.7941$$

Figure 1: Rotations to estimate the Jaccard index of a symmetry degree 8 shape. The original shape is filled with black and blue, the rotate one, in black and red.

$(0,d), (1,d+1), \ldots (d-1, k-1)$, since (d,k) coincides with the pair $(0,d)$ and then the pairs are reprocessed. The resulting transformation of the equation 2 is as follows:

$$J^{(k)}(A) = \begin{cases} \frac{2}{k(k-1)} \left(\sum_{i=1}^{\frac{k-1}{2}} k \frac{|A_0 \cap A_i|}{|A_0 \cup A_i|} \right), \\ \qquad\qquad\qquad\qquad \text{if } k \text{ is odd;} \\ \frac{2}{k(k-1)} \left(\left(\sum_{i=1}^{\frac{k}{2}-1} k \frac{|A_0 \cap A_i|}{|A_0 \cup A_i|} \right) + \frac{k}{2} \frac{|A_0 \cap A_{\frac{k}{2}}|}{|A_0 \cup A_{\frac{k}{2}}|} \right), \\ \qquad\qquad\qquad\qquad \text{if } k \text{ is even.} \end{cases} \quad (3)$$

Note that the sum of the coefficients in parentheses in the equation above equals to $\frac{k(k-1)}{2}$ in both cases.

The average Jaccard index estimation flow for rotated shapes is shown in Fig. 1. For exact symmetry, the focus point coincides with the center of gravity. For quasi-symmetric shapes, finding a focus point optimal in terms of Jaccard index is a separate problem. Note that for shapes with a sufficiently high symmetry measure, the focus is often close to the center of gravity. It prompts to limit the area of possible focus positions. The following section investigates the exact focus location problem.

3 UPPER JACCARD INDEX ESTIMATES BASED ON THE RADON TRANSFORM

Rotation, just like reflection, is a special case of a projective transformation that converts straight lines into

straight lines. We define lines by a two parameters (r,θ): line to the origin distance, and the angle between the normal to the line $(\cos\theta,\sin\theta)$ and the axis X. Such a line is defined by the equation

$$x\cos\theta + y\sin\theta = r. \tag{4}$$

We consider an affine transformation with the matrix

$$\mathbf{C} = \begin{bmatrix} c_{11} & c_{12} & c_{13} \\ c_{21} & c_{22} & c_{23} \\ 0 & 0 & 1 \end{bmatrix}, \quad \det\mathbf{C} \neq 0.$$

Note that this transformation converts $(-\sin\theta,\cos\theta)$, the directional vector of the line $l(r,\theta)$ into a vector

$$(-\lambda\sin\theta',\lambda\cos\theta') =$$
$$= (-c_{11}\sin\theta + c_{12}r\cos\theta, -c_{21}\sin\theta + c_{22}\cos\theta).$$

Therefore, the line $l(r,\theta)$ is converted into the line $l(r',\theta')$, where

$$\theta' = \operatorname{atan2}(c_{11}\sin\theta - c_{12}\cos\theta, -c_{21}\sin\theta + c_{22}\cos\theta),$$
$$r' = \cos\theta'(c_{11}r\cos\theta + c_{12}r\sin\theta + c_{13}) +$$
$$+ \sin\theta'(c_{21}r\cos\theta + c_{22}r\sin\theta + c_{23}). \tag{5}$$
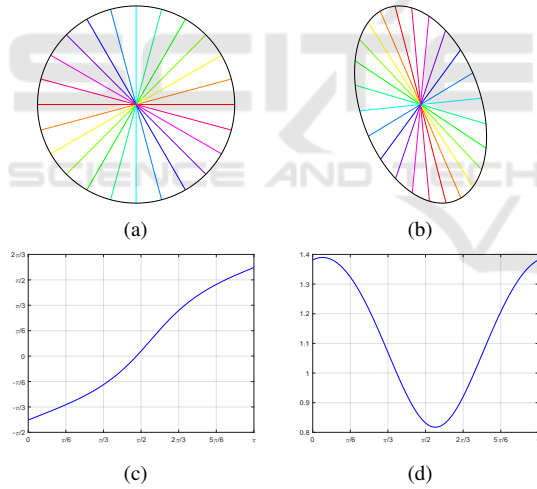

(a)

(b)

(c)

(d)

Figure 2: The lines before (a) and after (b) the affine transformation (color-coded). (c) $\theta'(\theta)$ and (d) $\lambda(\theta)$ curves.

Also note that under the transformation the distances along the parallel lines are scaled uniformly, regardless of position on the line. The scale factor is: $\lambda(\theta) = \sqrt{(-c_{11}\sin\theta + c_{12}\cos\theta)^2 + (-c_{21}\sin\theta + c_{22}\cos\theta)^2}$. It follows from the change in the directional vector length. Fig. 2 shows an example of the line affine transformation $\mathbf{C}$.

It may be possible to estimate the Jaccard index from the corresponding characteristics of the line before and after transformations. One of the most common such characteristics is the Radon transform. It

specifies the length of the intersection of all possible lines with a shape. It is expressed as

$$T_A(r,\theta) = \int\limits_{-\infty}^{+\infty} \chi_A(r\cos\theta - z\sin\theta, r\sin\theta + z\cos\theta)dz. \tag{6}$$

Where χ_A is the characteristic function of the shape A:

$$\chi_A(x,y) = \begin{cases} 1, & \text{if } (x,y) \in A; \\ 0, & \text{if } (x,y) \notin A. \end{cases} \tag{7}$$

The Radon transform gives natural upper estimates of the Jaccard index.

Theorem 2. Let the shape A' is obtained from A by an affine transformation. Let us denote $r'^{-1}(r,\theta)$ and $\theta'^{-1}(\theta)$ such r'' and θ'' that $r'(r,\theta'') = r$ and $\theta'(\theta'') = \theta$. Then for any given θ

$$|A \cap A'| \leq \int_{-\infty}^{+\infty} \min\left(T(r,\theta), \lambda(\theta'^{-1}(\theta))T(r'^{-1}(r,\theta), \theta'^{-1}(\theta))\right)dr = B^{\cap}(A), \tag{8}$$

$$|A \cup A'| \geq \int_{-\infty}^{+\infty} \max\left(T(r,\theta), \lambda(\theta'^{-1}(\theta))T(r'^{-1}(r,\theta), \theta'^{-1}(\theta))\right)dr = B^{\cup}(A). \tag{9}$$

Proof. Let us consider the intersection area expressed as an integral over the $l(r,\theta)$ lines when θ is fixed:

$$|A \cap A'| =$$
$$= \int\limits_{-\infty}^{+\infty}\int\limits_{-\infty}^{+\infty} \chi_A(x(r,\theta,z),y(r,\theta,z))\chi_{A'}(x(r,\theta,z),y(r,\theta,z))dzdr \leq$$
$$\leq \int\limits_{-\infty}^{+\infty} \min\left(T_A(r,\theta), T_{A'}(r,\theta)\right)dr, \tag{10}$$

where $x(r,\theta,z) = r\cos\theta - z\sin\theta$, $y(r,\theta,z) = r\sin\theta + z\cos\theta$.

Similarly,

$$|A \cup A'| \geq \int_{-\infty}^{+\infty} \max\left(T_A(r,\theta), T_{A'}(r,\theta)\right). \tag{11}$$

Since the line $l(r,\theta)$ is converted into the line $l(r',\theta')$ and the distances are stretched $\lambda(\theta)$ times,

$$T_{A'}(r',\theta') = \lambda(\theta)T_A(r,\theta),$$
$$T_{A'}(r,\theta) = \lambda(\theta'^{-1}(\theta))T_A(r'^{-1}(r,\theta), \theta'^{-1}(\theta)). \tag{12}$$

By substituting the expression for $T_{A'}(r,\theta)$, we obtain the sought equations. The theorem is now proved. $\square$

Since $|A'| = \det\mathbf{C}|A|$, $|A \cup A'| = |A| + |A'| - |A \cap A'|$,

$$\min\left(T_A(r,\theta), T_{A'}(r,\theta)\right) + \max\left(T_A(r,\theta), T_{A'}(r,\theta)\right) =$$
$$= T_A(r,\theta) + T_{A'}(r,\theta), \tag{13}$$

therefore, $B^{\cup}(A) + B^{\cap}(A) = (1 + \det\mathbf{C})|A|$. This results in the final upper estimate of the Jaccard index:

$$J(A) \leq \overline{J}(A) = \frac{B^{\cap}(A)}{(1 + \det\mathbf{C})|A| - B^{\cap}(A)}. \tag{14}$$

4 SEARCH FOR SYMMETRY FOCUS USING UPPER ESTIMATES

When we rotate a shape by the angle α, the $l(r,\theta)$ lines are converted into the $l(r',\theta+\alpha)$ lines. Let us first show that as shapes are rotated, the distance between the point projections along the corresponding lines is preserved. Note that the matrix of rotation about the point (x_c,y_c) is

$$\begin{bmatrix} \cos\alpha & -\sin\alpha & d_x \\ \sin\alpha & \cos\alpha & d_y \\ 0 & 0 & 1 \end{bmatrix},$$

where $d_x = -x_c\cos\alpha + y_c\sin\alpha + x_c$, $d_y = -x_c\sin\alpha - y_c\cos\alpha + y_c$.

Consider the points $a = (x_a, y_a)$ and $b = (x_b, y_b)$. Let their projections along the lines $l(r,\theta)$ are d away from each other:

$$x_b\cos\theta + y_b\sin\theta - x_a\cos\theta + y_a\sin\theta = d.$$

Then, after rotating by α, the distance between their projections along the $l(r,\theta+\alpha)$ lines will be the same:

$$\begin{aligned} &(x_b\cos\alpha - y_b\sin\alpha - x_c\cos\alpha + y_c\sin\alpha + x_c)\cos(\theta+\alpha) + \\ &+(x_b\sin\alpha + y_b\cos\alpha - x_c\sin\alpha - y_c\cos\alpha + y_c)\sin(\theta+\alpha) + \\ &-(x_a\cos\alpha - y_a\sin\alpha - x_c\cos\alpha + y_c\sin\alpha + x_c)\cos(\theta+\alpha) + \\ &-(x_a\sin\alpha + y_a\cos\alpha - x_c\sin\alpha - y_c\cos\alpha + y_c)\sin(\theta+\alpha) = \\ &=((x_b-x_a)\cos\alpha - (y_b-y_a)\sin\alpha)\cos(\theta+\alpha) + \\ &+((x_b-x_a)\sin\alpha + (y_b-y_a)\cos\alpha)\sin(\theta+\alpha) = \\ &=(x_b-x_a)(\cos\alpha\cos\theta\cos\alpha - \cos\alpha\sin\theta\sin\alpha) + \\ &+(x_b-x_a)(\sin\alpha\sin\theta\cos\alpha + \sin\alpha\cos\theta\sin\alpha) + \\ &+(y_b-y_a)(-\sin\alpha\cos\theta\cos\alpha + \sin\alpha\sin\theta\sin\alpha) + \\ &+(y_b-y_a)(\cos\alpha\sin\theta\cos\alpha + \cos\alpha\cos\theta\sin\alpha) = \\ &=(x_b-x_a)\cos\theta + (y_b-y_a)\sin\theta = d. \end{aligned}$$

Thus, r' is obtained from r by adding a value that depends on θ but not on r as the center of rotation is fixed:

$$\begin{aligned} d(\theta) &= ((x_a-x_c)\cos\alpha - (y_a-y_c)\sin\alpha + x_c)\cos(\theta+\alpha) + \\ &+ ((x_a-x_c)\sin\alpha + (y_a-y_c)\cos\alpha + y_c)\sin(\theta+\alpha) - x_a\cos\theta - y_a\sin\theta = \\ &= x_c\cos(\alpha+\theta) + y_c\sin(\alpha+\theta) - x_c\cos\theta - y_c\sin\theta = \\ &= x_c\left(2\sin\tfrac{\alpha+2\theta}{2}\sin\tfrac{-\alpha}{2}\right) + y_c\left(2\sin\tfrac{\alpha+2\theta}{2}\cos\tfrac{-\alpha}{2}\right) = \\ &= 2\sin\tfrac{\alpha+2\theta}{2}\left(x_c\cos\left(\tfrac{\pi}{2}+\tfrac{\alpha}{2}\right) + y_c\sin\left(\tfrac{\pi}{2}+\tfrac{\alpha}{2}\right)\right). \end{aligned} \tag{15}$$

As a result, all the centers of rotation on the $l(r, \frac{\pi}{2} + \frac{\alpha}{2})$ line produce an identical shift. We obtain $r'(r,\theta) = r + d(\theta)$, and since $\theta'^{-1}(\theta) = \theta - \alpha$, $r'^{-1}(r,\theta) = r - d(\theta-\alpha)$. Given that for a $\lambda(\theta) \equiv 1$ rotation, the equation 12 takes the form:

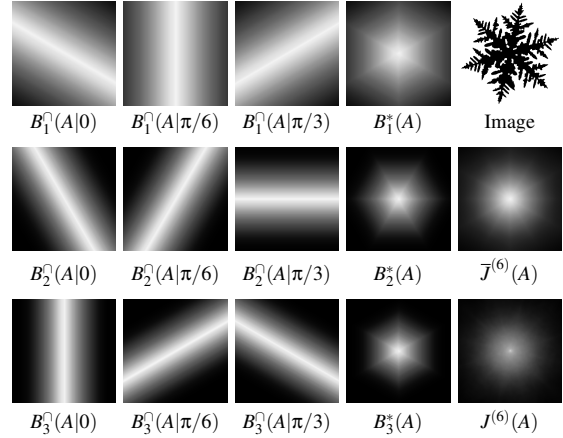$$T_{A'}(r,\theta) = T_A(r - d(\theta-\alpha), \theta - \alpha), \tag{16}$$

Figure 3: Upper Estimates of the Jaccard Index.

which results in a general upper estimate of the intersection, shown in Fig. 3.

$$B_i^{\cap}(A|\theta) = \int_{-\infty}^{+\infty} \min\left[T_A(r,\theta), T_A\left(r - d\left(\theta - \tfrac{2\pi i}{k}\right), \theta - \tfrac{2\pi i}{k}\right)\right] dr. \tag{17}$$

Note that the θ angle in these estimates is arbitrary, and $B_i^{\cap}(A|\theta) = B_i^{\cap}(A|\theta+\pi)$, since $T_A(r,\theta) = T_A(r,\theta+\pi)$. We will use θ from the $\{\frac{2\pi j}{k}\}_{j=0}^{k-1}$ set to refine the estimates taking into account all the rotation angles:

$$B_i^*(A) = \min_{0 \le j \le k-1}\{B_i^{\cap}(A|2\pi j/k)\}. \tag{18}$$

Therefore, we can express the final estimates for all the k images:

$$\overline{J}^{(k)}(A) = \begin{cases} \frac{2}{k-1}\sum_{i=1}^{\frac{k-1}{2}} \frac{B_i^*(A)}{2|A|-B_i^*(A)}, \\ \qquad\qquad\qquad\qquad \text{if } k \text{ is odd;} \\ \frac{1}{k-1}\left(\frac{B_{k/2}^*(A)}{2|A|-B_{k/2}^*(A)} + 2\sum_{i=1}^{\frac{k-1}{2}} \frac{B_i^*(A)}{2|A|-B_i^*(A)} \right), \\ \qquad\qquad\qquad\qquad \text{if } k \text{ is even.} \end{cases} \tag{19}$$

Note that so far the (x_c,y_c) center of rotation was assumed to be known, although the problem statement implies it is not. Let us denote the Jaccard index averaged over k images as by $J^{(k)}(A|x_c,y_c)$ for a rotation around the (x_c,y_c) point. Then we come to the following optimization problem:

$$\underset{x_c,y_c}{\text{maximize}}\ J^{(k)}(A|x_c,y_c).$$

To solve it, we apply the following algorithm with upper estimates:

1. Let the center of gravity of the A shape be the initial position of the (x^*, y^*) center of rotation.

2. Generate a list $L = \{(x,y)\,|\,(x,y)\, \in\, \text{conv}(A),\ \overline{J}^{(k)}(A|x,y)\, >\, J^{(k)}(A|x^*,y^*)\}$, and sort it in the descending by $\overline{J}^{(k)}(A|x,y)$ order.

3. Enumerate the L values while $\overline{J}^{(k)}(A|x,y) > J^{(k)}(A|x^*,y^*)$, calculate $J^{(k)}(A|x,y)$, replacing (x^*,y^*) with (x,y) if $J^{(k)}(A|x,y) > J^{(k)}(A|x^*,y^*)$.

5 ORDER OF SYMMETRY ESTIMATION USING THE FOURIER TRANSFORM OF THE SHAPE PROJECTION FEATURES

So far, the symmetry order k was assumed to be known, and was not questioned. An obvious approach would be to turn k into an optimization parameter:

$$\underset{k,x_c,y_c}{\text{maximize}}\, J^{(k)}(A|x_c,y_c) \equiv \underset{k}{\text{maximize}}\, \max_{x_c,y_c} J^{(k)}(A|x_c,y_c).$$

Let us note that a shape with an order k symmetry is also considered as symmetric with the m order, where m is the divisor of k. The problem statement above in some cases leads to giving the priority to one of the divisors if its symmetry measure is slightly higher. It does not agree well with the human concept of symmetry. A possible solution is to modify the estimates with the $R(v,k)$ regularization function which increases for both arguments:

$$\underset{k,x_c,y_c}{\text{maximize}}\, R\left(J^{(k)}(A|x_c,y_c),k\right),$$

or use the max divisor with the measure close to the max value as the degree of symmetry (Yip, 1999):

$$k^* = \max\{n : n \vdots \arg\max_k \max_{x_c,y_c} J^{(k)}(A|x_c,y_c),$$
$$\max_{x_c,y_c} J^{(n)}(A|x_c,y_c) \geq \mu \max_{k,x_c,y_c} J^{(k)}(A|x_c,y_c)\}.$$

However, such a solution still requires to search for the optimal focus for each order of symmetry. It would be computationally expensive. We used a fast order of symmetry estimation when the focus position is not known. Note that for a strictly symmetric shape with the k degree of symmetry its Radon transform is periodic:

$$T_A(r + d(\theta|x_c,y_c,2\pi/k), \theta + 2\pi/k) = T_A(r,\theta). \quad (20)$$

Therefore, $T_A(r, \theta + \frac{2\pi}{k})$ as a function of r is identical to $T_A(r,\theta)$ up to the shift value. We will describe the function with features independent of these shifts. A similar approach is also used to estimate the LIP-signature (Nguyen and Nguyen, 2018), where the following values are calculated: $\max_r T_A(r,\theta)$, $\int_{-\infty}^{+\infty}[T_A(r,\theta) > 0]dr$. They are invariant to shifts of r. Since the Fourier transform is well suited to detect the periodicity of a function, we use a single feature, a complex number:

$$W_A(\theta) = (T_{A,0.5}(\theta) - T_{A,0.5-\delta}(\theta)) + i(T_{A,0.5+\delta}(\theta) - T_{A,0.5}(\theta)), \quad (21)$$

where $T_{A,\gamma}(\theta)$ is the corresponding quantile of the A shape projections along the lines at the θ angle:

$$T_{A,\gamma}(\theta) = r, \text{ such that } \frac{1}{|A|}\int_{-\infty}^{r} T_A(s,\theta)ds = \gamma. \quad (22)$$

The $\mathcal{F}_A(k)$ discrete complex-valued Fourier transform is calculated for the $W_A(\theta) - \underset{\theta}{\text{mean}}\, W_A(\theta)$ function and then normalized:

$$\widehat{\mathcal{F}}_A(k) = \frac{\mathcal{F}_A(k)}{\sum_k (\mathcal{F}_A(k))^2}. \quad (23)$$

The final degree of symmetry is the max modulus amplitude:

$$k^* = \max_k |\widehat{\mathcal{F}}_A(k)|, \quad (24)$$

then the optimal center of rotation (x_c,y_c) is determined by the algorithm presented in the previous section.
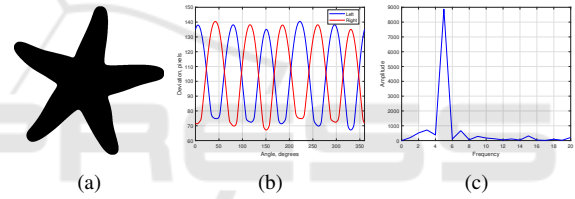

Figure 4: Image degree of symmetry estimation (a) with the Fourier transform (c) of the projection quantiles (b) for $\alpha = 0.25$.

Fig. 4 shows an example of determining the degree of symmetry with the proposed algorithm.

6 EXPERIMENTS

2 (19)   3 (8)   4 (23)   5 (5)   6 (16)   8 (21)

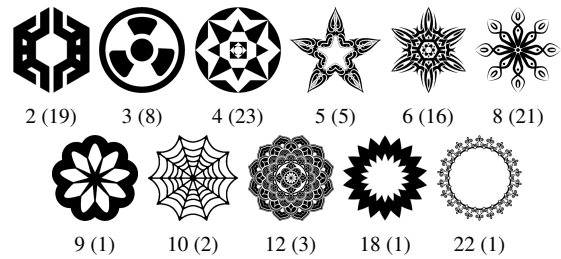9 (1)   10 (2)   12 (3)   18 (1)   22 (1)

Figure 5: UTLN-MRA dataset images. The number of images in the dataset is indicated in parentheses after the degree of symmetry.

The algorithm was implemented in C++ using Microsoft Visual Studio 2019 and the OpenCV 4.5.5 library. We ran it on a laptop with an Intel® Core™

i7-9750H CPU, 16 Gb RAM, and a NVIDIA GeForce GTX 1660 Ti video card. For comparison, we also implemented a Hough detector-based method which follows the concepts presented in (Yip, 1999). Since the search for symmetry in parallel projections is beyond the scope of this work, we skipped the projection parameter estimation step. We considered only the points that pass into each other after a "perfect" rotation. As a result, we produced Algorithm 1. It is worth mentioning how to scale the measure values for each degree of symmetry. Suppose we have an image with the k degree of symmetry. Then n of its pixels are split into $\frac{n}{k}$ orbits, each of which has $\frac{k(k-1)}{2}$ pairs of points that pass into each other after various rotations. Then, the maximum number of possible pairs is $\frac{n(k-1)}{2}$. If we divide the number of pairs found by this value, we get a fraction of the maximum. Note that the original paper proposes to consider only the boundary points of the image. We can assume the algorithm produces an approximate Jaccard index for these points.

We used the UTLN-MRA (Multiple Reflection Axis) image dataset presented in (Nguyen et al., 2022) and available at http://tpnguyen.univ-tln.fr/download/UTLN-Reflection/ to evaluate the efficiency of the proposed method. Although the dataset is originally designed to detect reflective symmetry, most images have multiple symmetry axes and the axes have a common point. Each image is divided by these axes into equal parts which can be transformed into each other by rotating the image around the common point. For this reason, the dataset is suitable for rotational symmetry experiments. The dataset contains 100 images. Their degree of symmetry, as evaluated by the authors, ranges from 2 to 22. Examples of the images with each degree of symmetry are shown in Fig. 5.
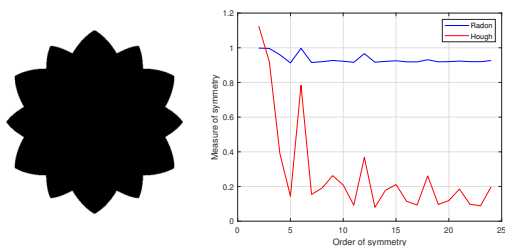

Figure 6: Comparison of the Radon transform and Hough detector-based methods.

Fig. 6 shows an example of the results for the proposed method based on the Radon transform and the method based on the Hough detector. Obviously, for both methods, the comparison of the estimates for different degrees of symmetry is complicated, especially

---

Algorithm 1: Search for rotational symmetry parameters.

Require: Image I
Ensure: The degree of symmetry k^* and its center (x^*, y^*)
  for $k = 2, \ldots, k_{max}$ **do**
    Fill the A accumulator array with zeros. The array size is the same as I
    for $t = 2, \ldots, k$ **do**
      for (p, q) from the set of all pairs formed by n boundary points of I **do**
        Define the affine similarity transformation T that converts the first point of a regular k-gon to p, and the t-th point, to q
        $(x, y) = T(0, 0)$ (the center point for a rotation which transforms p to q)
        Increment $A[\mathrm{int}(y), \mathrm{int}(x)]$
      end for
    end for
    Determine the k-symmetry center $(x_k, y_k) = \arg\max A$ and the symmetry measure $m_k = \frac{2 \max A}{n(k-1)}$
  end for
  Determine the center of symmetry (x^*, y^*) and the degree of symmetry k^* as the best value over all degrees.

---

if the "correct" degree is not a prime number. Note that the Hough-based method is more prone to overrate the estimates for smaller degrees of symmetry. Therefore, a more stringent regularization is required. By modifying the estimates according to the rule $R(v, k) = \frac{v}{1 + \lambda/k}$ the degree is correctly determined in 90% cases for the Hough detector (the optimal value $\lambda = 3.2$) and in 95% cases for the Radon transform-based method (the optimal value $\lambda = 0.28$).

The Fourier transform-based fast degree of symmetry estimation described in section 5 significantly reduces the run time and simplifies the regularizer selection. We will use it as follows. Since the differences characterizing the degree of symmetry can be found both at the edges and in the middle of a shape, we need to perform a quantile analysis across the entire $[0, 1]$ range. Therefore, we calculate the degree of symmetry $k(\delta)$ for multiple quantiles: $\delta \in \Delta = \{0.1, 0.2, 0.3, 0.4\}$, and the final degree is estimated as the argument of the max Jaccard index with regularization:

$$k^* = \arg\max_{k \in \{k(\delta) | \delta \in \Delta\}} \frac{J^{(k)}(A)}{1 + \lambda/k}. \tag{25}$$

This approach correctly determines the degree of symmetry for 98 of 100 images, while the total run time is reduced by two orders of magnitude: from 12 to 0.12 second on average per image. Note that without using a GPU, the Hough detector-based method

is about 10x slower than the Radon transform-based method without the fast degree of symmetry estimation. This is largely due to the presence of multiple contours in a number of images. For example, pay attention to the images with 5, 6, 8, 12, and 22 degrees of symmetry, that are shown in Fig. 5.
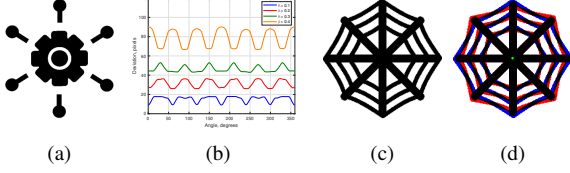

(a) (b) (c) (d)

Figure 7: Degree of symmetry estimation errors. (a) A 2 degree of symmetry image, (b) the quantiles of its Radon transform, (c) a 8 degree image, (d) its comparison with the imaged rotated by $45°$.

Let us conclude the study on this database with an error analysis. Fig. 7 shows the images for which the proposed method is unable to correctly determine the degree of symmetry. In the first case (Fig. 7ab) the shape in the image is a composition of symmetric shapes with the 6 and 8 orders of symmetry, and its degree of symmetry is equal to the greatest common divisor of these numbers: 2. A Fourier analysis does not identify that the shape is composite and predicts the degree of 6 for all the quantiles. In the second case (Fig. 7cd), the shape consists of thin elements that do not overlap well when rotated, although the human perception identifies 8 equal sections in the shape. As a result, the measure for degree 8 vs. degrees 2 and 4 drops too much to be corrected by the regularizer: 0.9012 vs. 0.9986 and 0.9988, respectively. The errors indicate that it is difficult to find a general symmetry measure for all shapes. When the shape is based on a wide circle, as in Fig. 6, the measures are close to each other for many degrees of symmetry, and the differences that distinguish the degree are expressed only in a small fraction of the Jaccard index. On the other hand, a shape formed by thin elements may poorly overlap itself after rotation. It makes us think about further modifications of the symmetry measure, such as using pixel weights and non-affine transforms.

Although the R and LIP signatures (Nguyen et al., 2022) are used to detect only reflection symmetry, they can be naturally adapted to analyze rotational symmetry. Recall that the R-signature is defined as follows:

$$R_A(\theta) = \int_{-\infty}^{+\infty} T_A^2(r, \theta) dr. \quad (26)$$

In turn, the LIP-signature is

$$L_A(\theta) = \frac{\max_r T_A(\theta, r)}{\sup\{R_+(\theta + \frac{\pi}{2})\} - \inf\{R_+(\theta + \frac{\pi}{2})\}}, \quad (27)$$

$$R_+(\theta) = \{r : T_A(\theta, r) > 0\}.$$

Note that for a figure with rotational symmetry of degree k, the corresponding signatures are periodic:

$$S_A\left(\theta + \tfrac{2\pi}{k}\right) = S_A(\theta), \quad S_A \in \{R_A, L_A\}. \quad (28)$$

It is on this property that our procedure for determining the quality measure of rotational symmetry will be based using correlation as in the original article:

$$\mathcal{G}_A(k) = \frac{1}{\lceil \frac{k}{2} \rceil - 1} \sum_{i=1}^{\lceil \frac{k}{2} \rceil - 1} \mathrm{corr}_{\theta \in [0, 2\pi]}\left(S_A(\theta), S_A(\theta + \tfrac{2\pi}{k})\right). \quad (29)$$

At the same time, these signatures are π-periodic by design, so $\mathrm{corr}_{\theta \in [0, 2\pi]}\left(S_A(\theta), S_A(\theta + \pi)\right) = 1$, and $\mathcal{G}_A(2k) = \mathcal{G}_A(k)$ if k is odd.
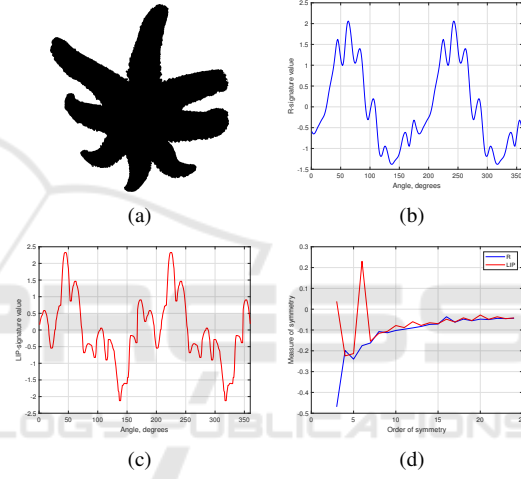

(a) (b)

(c) (d)

Figure 8: Detection of rotational symmetry using Nguyen signatures. (a) Initial image; (b) its R-signature; (c) its LIP-signature; (d) symmetry measures for various degrees.

For the final experiment, 57 binarized starfish images were prepared from the repositories available at https://australian.museum/learn/animals/sea-stars/sydney-seastars/ and http://www.jaxshells.org/starfish.htm. For each image, the number of rays per individual was manually determined, which varied from 5 to 11 in the entire set. The determination of the degree of symmetry was considered correct if the corresponding measure of symmetry based on signatures was among the four largest values. Note that this is a looser setting than in the method proposed by us, since it does not require identifying the best degree among the four in additional indicators. As a result, the number of individuals with correctly counted rays was 32 (56.14%) for the R-signature, 40 (70.18%) for the LIP-signature, and 49 (85.96%) when using proposed Fourier-based signature. This indicates that the Nguyen signatures, depicted in Fig. 8, are less

suitable for rotational symmetry detection, possibly due to the inability to distinguish directions at angles θ and $\theta + \pi$.

$J^{(7)}(A|x_c, y_c) = 0.7828$ $J^{(7)}(A|x^*, y^*) = 0.8381$

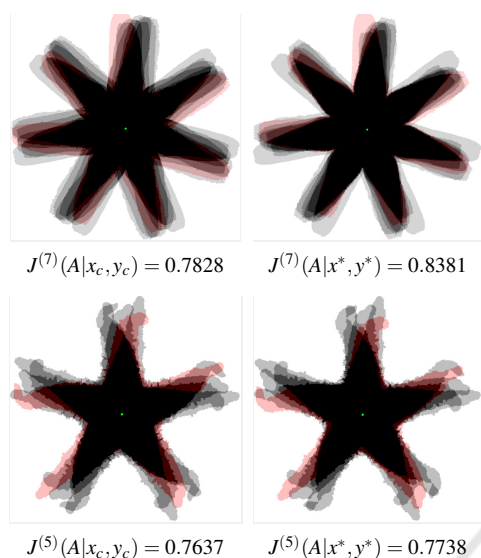$J^{(5)}(A|x_c, y_c) = 0.7637$ $J^{(5)}(A|x^*, y^*) = 0.7738$

Figure 9: Comparison of Jaccard measures at the center of mass (left column) and at the optimal point (right column). Images averaged over all rotations are shown. The original images are highlighted in red.

Finally, we note that for all images the center of symmetry found from the upper estimates of the Jaccard index coincides with the center found by complete enumeration. This is due to the very nature of the algorithm. It ensures that the optimal center point is not be excluded at the point filtering stage since the upper estimate is high, and eventually the symmetry measure for it will be explicitly checked. At the same time, the process of searching for the optimal focus can sometimes significantly improve the initial approximation in the form of the center of mass, but sometimes this approximation turns out to be quite successful (Fig. 9).

7 CONCLUSION

Finding reflective and rotational symmetry parameters is an optimization problem. Its solution has a significant computational cost, since it is reduced to comparing a group of images for each set of possible parameters. There is a need to develop a more efficient optimization algorithm. For example, the search space should be reduced. This study shows that for a preliminary estimation of the optimum it is sufficient to compare not the images, but the simplest statistical parameters of their projections which can be obtained with the Radon transform. It is shown that such sta-

tistical parameters are closely related to the Jaccard index extensively used for comparing the shapes in images since it directly produces the upper estimates for each measure.

It is assured that the number of image comparisons in a group can be significantly reduced by providing a suitable mathematical expression for the generalized Jaccard index. We presented a theoretical rationale for the proposed method. It is shown that its underlying principle is applicable to the analysis of many reflective and rotational symmetries expressed by affine transformations. We also developed an original fast algorithm based on the Fourier analysis of quantile distribution of the shape's pixel projections on various lines.

The experiments show that the proposed method is highly efficient which makes it suitable for real-time applications. It is better than the similar Hough transform-based method not only because it is an order of magnitude faster, but also because it is easier to interpret and more versatile. The method correctly identifies the degree of symmetry for almost any image, and the found center of symmetry is guaranteed to be the global maximum of the Jaccard index.

Further research may be focused on developing an efficient algorithm for affine transforms that are not similarity transforms, such as skews and stretchings.

ACKNOWLEDGEMENTS

REFERENCES

Aguilar, W., Alvarado-Gonzalez, M., Garduno, E., Velarde, C., and Bribiesca, E. (2020). Detection of rotational symmetry in curves represented by the slope chain code. *Pattern Recognition*, 107:107421.

Dieleman, S., De Fauw, J., and Kavukcuoglu, K. (2016). Exploiting cyclic symmetry in convolutional neural networks. In *Proceedings of the 33rd International Conference on Machine Learning - Volume 48*, ICML'16, pages 1889–1898. JMLR.org.

Kondra, S., Petrosino, A., and Iodice, S. (2013). Multi-scale kernel operators for reflection and rotation symmetry: Further achievements. In *IEEE Computer Society Conference on Computer Vision and Pattern Recognition Workshops*, pages 217–222.

Krippendorf, S. and Syvaeri, M. (2020). Detecting symmetries with neural networks. *Machine Learning: Science and Technology*, 2(1):015010.

Kushnir, O., Fedotova, S., Seredin, O., and Karkishchenko, A. (2017). Reflection symmetry of shapes based on skeleton primitive chains. *Communications in Computer and Information Science*, 661:293–304.

Lee, S. and Liu, Y. (2010). Skewed rotation symmetry group detection. *IEEE Transactions on Pattern Analysis and Machine Intelligence*, 32(9):1659–1672.

Lei, Y. and Wong, K. C. (1999). Detection and localisation of reflectional and rotational symmetry under weak perspective projection. *Pattern Recognition*, 32(2):167–180.

Llados, J., Bunke, H., and Marti, E. (1997). Finding rotational symmetries by cyclic string matching. *Pattern Recognition Letters*, 18(14):1435–1442.

Nguyen, T. P. (2019). Projection based approach for reflection symmetry detection. In *2019 IEEE International Conference on Image Processing (ICIP)*, pages 4235–4239.

Nguyen, T. P. and Nguyen, X. S. (2018). Shape measurement using LIP-signature. *Computer Vision and Image Understanding*, 171:83–94.

Nguyen, T. P., Truong, H. P., Nguyen, T. T., and Kim, Y.-G. (2022). Reflection symmetry detection of shapes based on shape signatures. *Pattern Recognition*, 128:108667.

Seredin, O., Liakhov, D., Kushnir, O., and Lomov, N. (2022). Jaccard index-based detection of order 2 rotational quasi-symmetry focus for binary images. *Pattern Recognition and Image Analysis*, 32(3):672–681.

Shiv Naga Prasad, V. and Davis, L. (2005). Detecting rotational symmetries. In *Tenth IEEE International Conference on Computer Vision (ICCV'05) Volume 1*, volume 2, pages 954–961.

Yip, R. K. (1999). A Hough transform technique for the detection of parallel projected rotational symmetry. *Pattern Recognition Letters*, 20(10):991–1004.

Yip, R. K. (2007). Genetic Fourier descriptor for the detection of rotational symmetry. *Image and Vision Computing*, 25(2):148–154. Soft Computing in Image Analysis.